Loss-Induced Omnidirectional Bending to the Normal in ϵ-Near-Zero Metamaterials

Simin Feng

Phys. Rev. Lett. **108**, 193904 — Published 10 May 2012

DOI: 10.1103/PhysRevLett.108.193904

Loss-Induced Omnidirectional Bending to the Normal in ϵ-near-Zero Metamaterials

Simin Feng[1,*]

[1]*Michelson Lab, Physics Division, Naval Air Warfare Center, China Lake, California 93555*

Contrary to conventional wisdom that light bends away from the normal when it passes from high to low refractive index media, here we demonstrate an exotic phenomenon that the direction of electromagnetic power can bend towards the normal when light is incident from an arbitrary high refractive index medium (or air) to ϵ-near-zero (ENZ) metamaterial. Moreover, the direction of the transmission is close to the normal for all angles of incidence. This anti-Snell's law refraction is resulted from the interplay between ENZ and material loss. The loss can increase the transmission at the air-ENZ interface and collimate the beam inside the ENZ medium. Furthermore, in an ideal loss configuration, the propagation loss in anisotropic ENZ materials can approach zero when the material loss goes to infinity.

PACS numbers: 42.25.Bs, 42.79.Wc, 78.67.Pt

Bending of light towards the normal when it passes from low to high refractive index media is one of the fundamental phenomena in optics. As a manifestation of this phenomenon, directive emission into air by a source inside the material with vanishingly small permittivity, known as ϵ-near-zero (ENZ) metamaterials, was demonstrated recently [1]. ENZ materials have gained prominence as useful components to guide light and alter radiations [2–6]. Previous studies on ENZ-directive emission have been focused on the radiation from low ($\epsilon \approx 0$) to high (air) refractive index media [1, 7–11], where the directive transmission can be understood from Snell's law that dictates the light bending to the normal. From the reciprocal theorem, for the radiation from high to low refractive index media, the transmitted beam should spread out in grazing angles as the result of bending away from the normal. Contrary to this conventional behavior, in this paper we will show that the electromagnetic (EM) power can bend towards the normal when passing from arbitrary high ($\epsilon_1 \gg 1$) to low ($\epsilon_2 \approx 0$) refractive index media as shown in Fig. 1a – anti-Snell's law refraction. Moreover, the direction of the transmission is close to the normal for all angles of incidence. Unlike negative refraction [12], this anti-Snell's law refraction is induced by material loss. The interplay between ENZ and loss leads to unusual wave interaction. This phenomenon is fundamentally different from the spatial filter effect previously studied in the lossless ENZ slab [11] which, in the limit of $\epsilon = 0$, allows zero spatial frequency (normal incidence) for total transmission, but reflects oblique incidences. EM properties in lossy ENZ media are unconventional and counterintuitive. Material loss can switch a broadband reflection to a broadband transmission, and then bend all spatial components to the normal. Moreover, the transmission at the air-ENZ interface increases with the loss. Interestingly, for a certain ideal loss design, the collimated beam can propagate indefinitely in the anisotropic ENZ medium when the loss approaches infinity.

This refraction and propagation anomaly may be useful for projecting EM power into one direction as shown in Fig. 1b, where the waves from all directions bend to the normal upon entering the ENZ material. A plasmonic thin-film is superimposed on the ENZ medium to enhance the transmission through structural resonances. Regardless of the incidence angles, the transmitted powers can impinge normally to the receptors or photocells embedded in the ENZ medium, which increase the acceptance angle and energy transfer.

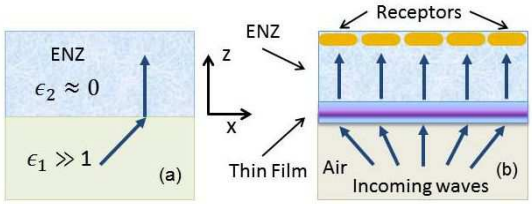

FIG. 1. (Color online) (a) A plane wave is incident from arbitrary high permittivity ($\epsilon_1 \gg 1$) medium to ENZ ($\epsilon_2 \approx 0$) metamaterial. (b) Incoming waves in air from different directions all bend to the normal upon entering the ENZ medium. A nanoplasmonic thin film is superimposed on the ENZ material to enhance the transmission. Receptors or photocells are embedded in the ENZ metamaterial.

Our derivation is based on anisotropic media. The results can be applied to isotropic materials. Assuming a harmonic time dependence $\exp(-i\omega t)$ for the EM field, from Maxwell's equations, we have

$$\begin{aligned} \nabla \times (\bar{\bar{\mu}}_n^{-1} \cdot \nabla \times \boldsymbol{E}) &= k_0^2 (\bar{\bar{\epsilon}}_n \cdot \boldsymbol{E}), \\ \nabla \times (\bar{\bar{\epsilon}}_n^{-1} \cdot \nabla \times \boldsymbol{H}) &= k_0^2 (\bar{\bar{\mu}}_n \cdot \boldsymbol{H}), \end{aligned} \tag{1}$$

where $k_0 = \omega/c$; and the $\bar{\bar{\epsilon}}_n$ and $\bar{\bar{\mu}}_n$ are, respectively, the permittivity and permeability tensors for each uniform region ($n = 1, 2, \cdots$), which in the principal coordinates can be described by $\bar{\bar{\epsilon}}_n = \epsilon_{nx}\hat{\boldsymbol{x}}\hat{\boldsymbol{x}} + \epsilon_{ny}\hat{\boldsymbol{y}}\hat{\boldsymbol{y}} + \epsilon_{nz}\hat{\boldsymbol{z}}\hat{\boldsymbol{z}}$ and $\bar{\bar{\mu}}_n = \mu_{nx}\hat{\boldsymbol{x}}\hat{\boldsymbol{x}} + \mu_{ny}\hat{\boldsymbol{y}}\hat{\boldsymbol{y}} + \mu_{nz}\hat{\boldsymbol{z}}\hat{\boldsymbol{z}}$, respectively. Consider transverse magnetic (TM) modes, corresponding to non-zero field components H_y, E_x, and E_z. The magnetic field H_y satisfies the following wave equation:

$$\frac{1}{\epsilon_z}\frac{\partial^2 H_y}{\partial x^2} + \frac{1}{\epsilon_x}\frac{\partial^2 H_y}{\partial z^2} + k_0^2 \mu_y H_y = 0, \tag{2}$$

which permits solutions of the form $\psi(z)\exp(i\beta x)$. Here the transverse wave number β is determined by the incident wave, and is conserved across the interface of different regions,

$$\beta^2 = k_0^2 \epsilon_{nz}\mu_{ny} - \alpha_n^2 \frac{\epsilon_{nz}}{\epsilon_{nx}}, \qquad (n = 1, 2, \cdots), \tag{3}$$

where α_n is the wave number in the z direction. The functional form of $\psi(z)$ is either a simple exponential $\exp(i\alpha_n z)$ for the semi-infinite regions or a superposition of $\cos(\alpha_n z)$ and $\sin(\alpha_n z)$ terms for the bounded regions along the z direction. The other two components E_x and E_z can be solved from H_y using Maxwell's equations. By matching boundary conditions at the interfaces, i.e., the continuity of H_y and E_x, the EM field can be derived in each region; and then the Poynting vector $\boldsymbol{S}$ can be computed from $\boldsymbol{S} = \Re(\boldsymbol{E} \times \boldsymbol{H}^*)$. In anisotropic materials, the direction of the Poynting vector is different from that of the phase front of the field. Here, only the direction of the Poynting vector is considered since it is associated with the energy transport. The angle (θ_S) of the Poynting vector is measured from the Poynting vector to the surface normal, and is given by $\theta_S = \tan^{-1}(S_x/S_z)$. In Fig. 1a, the input medium is isotropic material with permittivity ϵ_1; the output medium is ENZ material ($\epsilon_2 \approx 0$). In the following, both anisotropic ($\epsilon_{2x} \neq \epsilon_{2z}$) and isotropic ($\epsilon_{2x} = \epsilon_{2z}$) ENZ materials will be considered. Figure 2 illustrates the effect of loss of the ENZ-materials on the transmission angle (TA) plotted against angle of incidence (AOI) with and without loss for different permittivity (ϵ_1) of the input medium. In the top panels, when the loss is zero ($\Im(\epsilon_{2z}) = 0$), the TA is 90 degree (grazing angle) except for the normal incidence. This behavior is complied with Snell's law. In the bottom panels, with a moderate loss $\Im(\epsilon_{2z}) = 0.6$, the TA switches to the near zero (the normal direction) for all AOI. This switching phenomenon persists even for the much higher permittivity ($\epsilon_1 = 100$) of the input medium (middle and right panels).

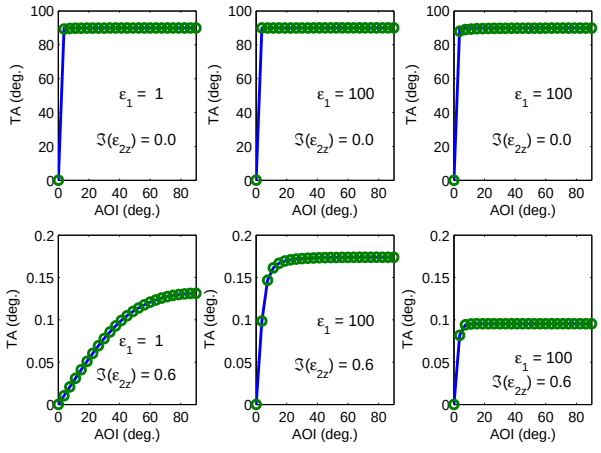

FIG. 2. (Color online) TA of the Poynting vector versus AOI when $\epsilon_{2z} = 0.001 + i\epsilon^i_{2z}$. Left and middle panels: anisotropic ENZ material with $\epsilon_{2x} = 1$. Right panels: isotropic ENZ material with $\epsilon_{2x} = \epsilon_{2z}$. Top panels: $\epsilon^i_{2z} = 0$. Bottom panels: $\epsilon^i_{2z} = 0.6$. Left panels: $\epsilon_1 = 1$. Middle and right panels: $\epsilon_1 = 100$. A good agreement between the numerical (blue-solid) and analytical (green-circles) results. Material loss switches the TA from the grazing angle 90° (top panels) to the near-zero angle (bottom panels) for all AOI.

To understand this loss-induced switching behavior, let's analyze the transmission angle (θ_S), which is given by

$$\tan(\theta_S) = \frac{S_x}{S_z} = \frac{\Re\left(\dfrac{\bar{\beta}}{\epsilon_{2z}}\right)}{\Re\left[\sqrt{\dfrac{\mu_{2y}}{\epsilon_{2x}} - \dfrac{(\bar{\beta})^2}{\epsilon_{2x}\epsilon_{2z}}}\right]}, \tag{4}$$

where $\bar{\beta} \equiv \beta/k_0$, and $\bar{\beta}$ (real) is determined by the incidence angle. The transmission angle of the Poynting vector depends only on the input and output media. In the case of $\epsilon_{2x} \to 0$ and ϵ_{2z} finite, Eq. (4) indicates $\theta_S \to 0°$ (normal direction). For the case of $\epsilon_{2z} \to 0$ and ϵ_{2x} finite and the case of isotropic ENZ material with $\epsilon_{2x} = \epsilon_{2z} \to 0$, the analysis is more involved. The numerator of Eq. (4) can be written as

$$\Re\left(\frac{\bar{\beta}}{\epsilon_{2z}}\right) = \frac{\bar{\beta}\,\epsilon^r_{2z}}{|\epsilon_{2z}|^2}, \tag{5}$$

where $\epsilon^r_{2z} \equiv \Re(\epsilon_{2z})$. Assuming μ_{2y} is real, the denominator of Eq. (4) becomes

$$\Re\left[\sqrt{\frac{\mu_{2y}}{\epsilon_{2x}} - \frac{(\bar{\beta})^2}{\epsilon_{2x}\epsilon_{2z}}}\right] = \frac{a\bar{\beta}}{|\epsilon_{2x}\epsilon_{2z}|}, \tag{6}$$

where

$$a^2 = \frac{1}{2}\left(A\epsilon^r_{2x} + B|\epsilon_{2x}| - \epsilon^r_{2x}\epsilon^r_{2z} + \epsilon^i_{2x}\epsilon^i_{2z}\right), \tag{7}$$

where $\epsilon^i_{2z} \equiv \Im(\epsilon_{2z})$, $\epsilon^r_{2x} \equiv \Re(\epsilon_{2x})$, $\epsilon^i_{2x} \equiv \Im(\epsilon_{2x})$, and

$$A \equiv \frac{|\epsilon_{2z}|^2\mu_{2y}}{(\bar{\beta})^2}, \quad B = \sqrt{|\epsilon_{2z}|^2 - 2A\epsilon^r_{2z} + A^2}. \tag{8}$$

Thus, the transmission angle (θ_S) becomes

$$\tan(\theta_S) = \frac{|\epsilon_{2x}|\epsilon^r_{2z}}{a\,|\epsilon_{2z}|}. \tag{9}$$

The loss-induced angular switch observed in Fig. 2 can be explained from Eq. (9). For the anisotropic medium $\epsilon_{2x} \neq \epsilon_{2z}$ and ϵ_{2x} is finite, if $\epsilon^i_{2z} = 0$, when $\epsilon^r_{2z} \to 0$, $\epsilon^r_{2z}/|\epsilon_{2z}| \to 1$ and $a \to 0$, thus $\theta_S \to 90°$. If $\epsilon^i_{2z} \neq 0$, when $\epsilon^r_{2z} \to 0$, $\epsilon^r_{2z}/|\epsilon_{2z}| \to 0$ and a is finite, thus $\theta_S \to 0°$. On the other hand, if ϵ_{2z} is finite, when $\epsilon_{2x} \to 0$, $a \to \sqrt{\epsilon_{2x}}$, thus $\theta_S \to 0°$. For the isotropic case, let $\epsilon_{2x} = \epsilon_{2z} \equiv \epsilon^r_2 + i\epsilon^i_2$. If $\epsilon^i_2 = 0$, when $\epsilon^r_2 \to 0$, $\epsilon^r_{2z}/|\epsilon_{2z}| \to 1$ and $a \to (\epsilon^r_2)^{3/2}$, thus $\theta_S \to 90°$. If $\epsilon^i_2 \neq 0$, when $\epsilon^r_2 \to 0$, $\epsilon^r_{2z}/|\epsilon_{2z}| \to 0$ and a is finite, therefore $\theta_S \to 0°$. Equation (9) indicates when ϵ_{2z} is finite, both the real and imaginary of ϵ_{2x} should approach zero in order for $\theta_S \to 0°$. To validate Eq. (9), in Fig. 2 the TAs calculated from Eq. (9) (green-circles) are compared to those computed numerically (blue-solid), showing a perfect agreement.

A detailed investigation on the influence of the loss on the TA is presented in Supplemental Material [13]. In essence, the TA decreases with increasing the loss $\Im(\epsilon_{2z})$ and decreasing

the $\Re(\epsilon_{2z})$. When the $\Re(\epsilon_{2z}) \to 0$, the angular width of the transmission can be estimated from

$$\Delta\theta_S \approx \begin{cases} \dfrac{\sqrt{2}\,|\epsilon_x|\,\epsilon_z^r}{|\epsilon_z|^{3/2}\sqrt{|\epsilon_x| + \epsilon_x^i + \eta\,\epsilon_x^r}}, & \text{if } \eta \le 1 \\ \dfrac{\sqrt{2}\,|\epsilon_x|\,\epsilon_z^r}{|\epsilon_z|^{3/2}\sqrt{\epsilon_x^i + \eta(|\epsilon_x| + \epsilon_x^r)}}, & \text{if } \eta \ge 1 \end{cases}, \qquad (10)$$

where $\eta \equiv \dfrac{|\epsilon_z|\mu_y}{\epsilon_1\mu_1}$, and the subscript 2 in the ϵ_x, ϵ_z, and μ_y was omitted in above equation.

Not only can the loss omni-directionally switch the TA from the grazing to the normal, but also it can increase the transmission amplitude. Without loss, the huge mismatched impedance prevents EM waves from entering the medium. This picture changes dramatically with the loss. In fact, loss can mitigate the mismatch, thus increases the transmission. Figure 3 shows the transmittance of a plane wave incident from air to the ENZ medium. Clearly, material loss provides a mechanism for the EM power to enter the "door", switching a broadband reflection to a broadband transmission.

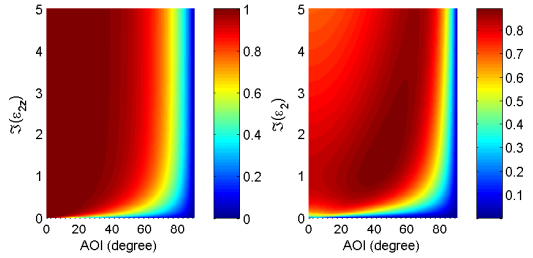

FIG. 3. (Color online) Transmittance at the air-ENZ interface vs. AOI and loss. Left panel: $\Re(\epsilon_{2z}) = 0.001$ and $\epsilon_{2x} = 1$. Right panel: $\epsilon_{2x} = \epsilon_{2z} = \epsilon_2$ and $\Re(\epsilon_2) = 0.001$. Color bars represent the magnitude of the transmittance. Note the transmission is zero when $\Im(\epsilon_{2z}) = 0$.

Moreover, some material loss can increase the propagation distance in anisotropic ENZ materials. Note the propagation constant in the z-direction, from Eq. (3), is given by

$$k_z \equiv \alpha = \sqrt{k_0^2\epsilon_x\mu_y - \frac{\epsilon_x}{\epsilon_z}\beta^2}\,. \qquad (11)$$

For the fixed ϵ_x, a higher loss in ϵ_z means a smaller $\Im(k_z)$, and thus a longer propagation for oblique incident beams since waves propagate mostly along the z-direction once inside the ENZ medium. Thus, if the loss in ϵ_x can be kept small, than the loss in ϵ_z is, in fact, favored for propagation. As $|\epsilon_z| \to \infty$, $\Im(k_z) \to \sqrt{(|\epsilon_x| - \epsilon_x^r)/2}$ [14]. The attenuation is limited by the $\Im(\epsilon_x)$. Figure 4 shows the influence of loss on propagation. Left panels present the normalized transmission vs. AOI at different propagation distances inside the anisotropic ENZ medium with different loss $\Im(\epsilon_z)$. The left-bottom panel indicates the transmission increases with the increase of the loss $\Im(\epsilon_{2z})$ and is eventually saturated (the curves for $\epsilon_{2z} = 3$ and $\epsilon_{2z} = 20$ are on top of each other). A broadband spatial frequency can enter the ENZ medium with more than 90% transmission for an angular bandwidth up to 50 degree and more than 50% for up to 75 degree. As the wave propagates inside the anisotropic ENZ medium, the power coming from non-zero AOI is gradually absorbed except for the normal incidence (see left-middle and left-top panels). This process is in fact quite opposite to what occurs in the lossless ENZ slab which, in the limit of $\epsilon = 0$, only allows the normal spatial component for total transmission due to Fabry-Perot resonance [11]. A lossless ENZ slab acts as a spatial filter [11], not a collimator. Whereas a lossy air-ENZ interface behaves as a collimator since most spatial components can pass the interface almost in parallel. Ideally, the wave can propagate indefinitely without decay if the loss $\Im(\epsilon_z) \to \infty$ and the loss $\Im(\epsilon_x) = 0$. Physically, it can be understood that ϵ_z is important for matching at the interface, but once the wave enters the material it propagates mostly along the normal, so the electric field 'feels' only the x-component of the permittivity. In essence, when the $|\epsilon_z|$ increases, the impact of the ϵ_z on wave propagation diminishes as the result of decreasing TA [14]. Propagation of the normalized total power in the ENZ medium is shown on the right panels of Fig. 4. When $\Im(\epsilon_{2z}) = 20$ (top panel), about 60% power is remained after a propagation of 5λ. For practical implementation, ENZ slab is more useful. In the anisotropic ENZ material, the z-component of the wave-vector, which is given by Eq. (11), is *not* zero when $\epsilon_x \neq 0$. Reflection from the second boundary of the ENZ slab can introduce interference and Fabry-Pérot effects. Hence, it is important to understand the behavior of output power of the anisotropic lossy ENZ slab (see Supplemental Material [15]). Note that the flat wavefront occurs only inside the ENZ ma-

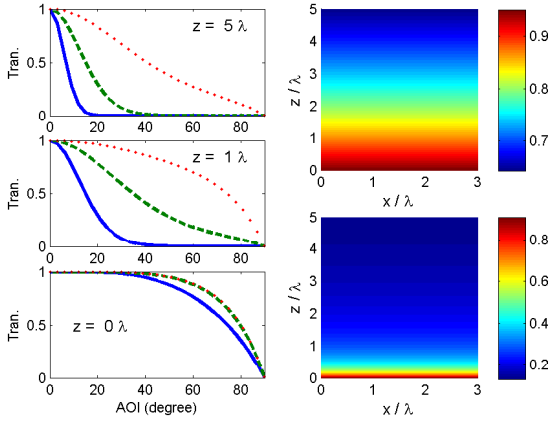

FIG. 4. (Color online) Left panels: Normalized transmitted power (by the input power for each AOI) inside the ENZ medium vs. AOI at the air-ENZ interface ($z = 0$, bottom panel), at the propagation distance $z = \lambda$ (middle panel) and $z = 5\lambda$ (top panel). Blue solid: $\Im(\epsilon_{2z}) = 0.6$. Green dashed: $\Im(\epsilon_{2z}) = 3$. Red dots: $\Im(\epsilon_{2z}) = 20$. $\Re(\epsilon_{2z}) = 0.001$ and $\epsilon_{2x} = 1$. No propagation decay for the normal incidence since $\beta = 0$ in Eq. (11). Right panels: Propagation of the normalized total power (integrating over AOI) in the ENZ medium. Top panel: $\Im(\epsilon_{2z}) = 20$. Bottom panel: $\Im(\epsilon_{2z}) = 0.6$.

terial. When the power comes out of the medium into air, the wavefront will return to the original form due to the conservation of parallel wave vector β. This result is different from the lossless ENZ slab where the wavefront keeps flat in air [11] since in their case the tilted wavefronts can never get into the material in the first place. It is well-known that many fascinating effects diminish due to the high loss of metamaterials. However, the material loss here can play a positive role, which collimates the beam and increases the transmission and propagation inside the ENZ medium.

Above EM properties may have many applications, such as directive antennas. Instead of radiation, we will explore this effect from a receiving perspective, i.e., redirect the EM power coming from different directions to the direction of the receivers to enhance the acquisition power, as shown in Fig. 1b. To increase the coupling, a matching coating can be deposited on the surface of the ENZ material such that the effective impedance of the overall structure is matched to that of air. For simplicity, we used a dielectric-metal-dielectric coating. With proper thicknesses, this sandwich structure can possess nearly-flat dispersion (omnidirectional resonance) [16, 17] due to coupled surface plasmon from closely spaced two dielectric-metal interfaces. By varying the thickness of each layer, the resonant frequency can be tuned. In our simulation, the materials of the dielectric and metallic layers are, respectively, amorphous polycarbonate (APC) and silver (Ag). The refractive index of the APC is given by [18] $n_p = 1.5567 + 8.0797\times10^{-3}/\lambda^2 + 3.5971\times10^{-4}/\lambda^4$, where λ is the wavelength in μm. The loss of the APC is very small, and thus neglected. Absorption of Ag is included via the complex permittivity given from Palik [19].

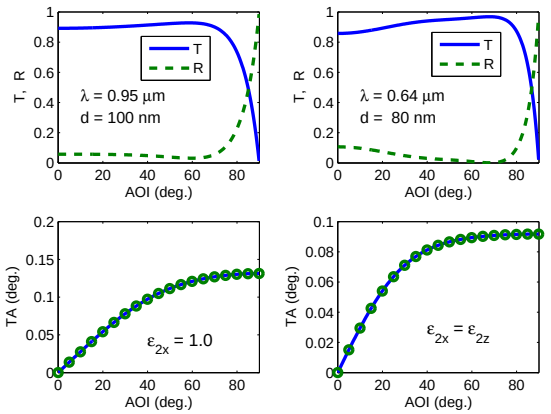

FIG. 5. (Color online) Top panels: Transmittance (blue-solid) and reflectance (green-dashed) of the APC-Ag-APC thin film vs. AOI when the back of the film is ENZ medium with $\epsilon_{2x} = 1$ (left panels) and $\epsilon_{2x} = \epsilon_{2z}$ (right panels). $\epsilon_{2z} = 0.001 + 0.6i$ for both. Bottom panels: corresponding transmission angle of the APC-Ag-APC film computed numerically (blue-solid) and analytically (green-circles), showing a perfect agreement. The thickness of Ag is 10 nm.

Figure 5 shows the transmittance and reflectance (top panels) of a plane wave incident from air to the APC-Ag-APC thin film, along with the corresponding TA (bottom panels). At the resonance, the thickness of the APC is $d = 100\,\text{nm}$ and the resonant wavelength $\lambda = 0.95\,\mu\text{m}$ for the anisotropic ENZ medium (left panels); and $d = 80\,\text{nm}$ and $\lambda = 0.64\,\mu\text{m}$ for the isotropic ENZ medium (right panels). About 90% transmission (top panels) is achieved for the AOI up to 70° with nearly-collimated beam in the normal direction (bottom panels). Compared with the case without the matching film (see left-bottom panel of Fig. 4), the angular bandwith is increased by 40%. A 2D plot showing the transmittance of the APC-Ag-APC coating as a function of AOI and wavelength is given in Supplemental Material [20]. Note the loss of the ENZ medium was not included when calculating the transmittance, which was computed right after the APC-Ag-APC, i.e., before traveling through the ENZ medium. If the receptors are embedded very close to the back of the film, the propagation loss in the ENZ medium can be minimized. On the other hand, by designing the anisotropic loss, $\Im(\epsilon_x) \approx 0$ and $\Im(\epsilon_z) \gg 0$, the propagation distance can be increased.

In conclusions, we have demonstrated the counterintuitive anti-Snell's law refraction and the loss-assisted transmission and propagation in ENZ materials. These results are sensitive to polarization and usually narrow band due to frequency dispersion. Nevertheless, these unconventional effects may find applications in communications, directive antennas, detectors, and sensors to increase acceptance angle and energy deliver without using optical lenses and mechanical gimbals. The concept of using anisotropic loss to control the direction and transmission brings a positive perspective to material loss and may open up a new avenue for metamaterial designs.

The author gratefully thanks the referees for their valuable suggestions and insightful comments. This work is sponsored by ONR's N-STAR and NAVAIR's ILIR programs.

* simin.feng@navy.mil

[1] S. Enoch, *et al.*, Phys. Rev. Lett. **89**, 213902 (2002).
[2] M. G. Silveirinha and N. Engheta, Phys. Rev. Lett. **97**, 157403 (2006).
[3] R. Liu, *et al.*, Phys. Rev. Lett. **100**, 023903 (2008).
[4] K. Halterman, S. Feng, and V. C. Nguyen, Phys. Rev. B **84**, 075162 (2011).
[5] D. C. Adams, *et al.*, Phys. Rev. Lett. **107**, 133901 (2011).
[6] V. Mocella, *et al.*, Phys. Rev. Lett. **102**, 133902 (2009).
[7] R. W. Ziolkowski, Phys. Rev. E **70**, 046608 (2004).
[8] Y. Yuan, *et al.*, Phys. Rev. A **77**, 053821 (2008).
[9] Y. Jin and S. He, Opt. Express **18**, 16587 (2010).
[10] G. Lovat, *et al.*, IEEE Trans. Antennas Propag. **54**, 1017 (2006).
[11] A. Alù, *et al.*, Phys. Rev. B **75**, 155410 (2007).
[12] R. A. Shelby, D. R. Smith, S. Schultz, Science **292**, 77 (2001).
[13] See Figs. 1 and 2 in Supplementary Material.
[14] See Eq. (1) and discussion in Supplementary Material.
[15] See Figs. 3, 4, 5, and discussion in Supplementary Material.
[16] H. Shin, *et al.*, Appl. Phys. Lett. **84**, 4421 (2004).
[17] J. Zhang, *et al.*, J. Opt. Soc. Am. B **25**, 1474 (2008).
[18] M. J. Roberts, *et al.*, J. Nanophoton. **4**, 043511 (2010).
[19] E. D. Palik, *Handbook of Optical Constants of Solids* (Academic, San Diego, 1998).

[20] See Fig. 6 in Supplementary Material.